NJC

Accepted Manuscript

This is an *Accepted Manuscript*, which has been through the Royal Society of Chemistry peer review process and has been accepted for publication.

Accepted Manuscripts are published online shortly after acceptance, before technical editing, formatting and proof reading. Using this free service, authors can make their results available to the community, in citable form, before we publish the edited article. We will replace this *Accepted Manuscript* with the edited and formatted *Advance Article* as soon as it is available.

You can find more information about *Accepted Manuscripts* in the Information for Authors.

Please note that technical editing may introduce minor changes to the text and/or graphics, which may alter content. The journal's standard Terms & Conditions and the Ethical guidelines still apply. In no event shall the Royal Society of Chemistry be held responsible for any errors or omissions in this *Accepted Manuscript* or any consequences arising from the use of any information it contains.

ROYAL SOCIETY OF CHEMISTRY

www.rsc.org/njc

A highly sensitive electrochemical DNA sensor was constructed by homogenously distributing Au nanoparticles (AuNPs) on flower-like 3D ZnO superstructures- chitosan (CS) matrix.

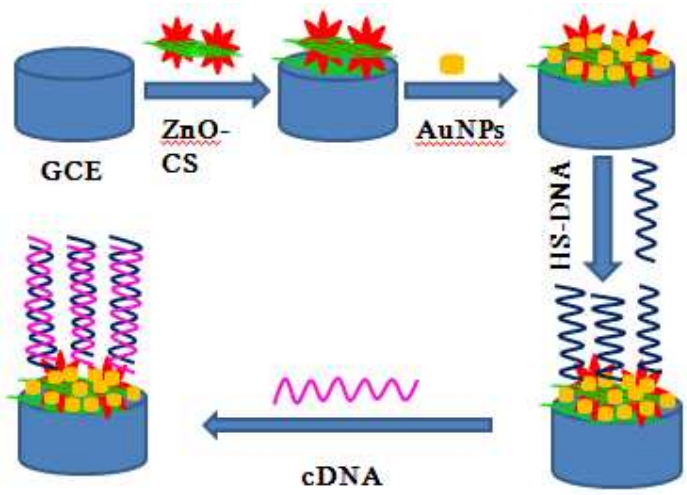

A label-free electrochemistry biosensor based flower-like 3-dimensional ZnO superstructures for detection of DNA arrays

Linxia Fang[a,b], Kejing Huang[b], Baoling Zhang[a], Yujie liu[b], Qiuyu Zhang[a,*]

[a]*Department of Applied Chemistry, School of Science, Northwestern Polytechnical University, 710072 Xi'an, China*

[b]*College of Chemistry and Chemical Engineering, Xinyang Normal University, 464000 Xinyang ,China*

* Corresponding author. Tel: +86 13152160629
E-mail address: qyzhang@nwpu.edu.cn

Abstract

A novel label-free DNA hybridization biosensor was fabricated using flower-like 3-dimensional (3D) ZnO superstructures as enhanced sensing platform, employing chitosan (CS) as film-forming material. A highly sensitive electrochemical DNA sensor was constructed by homogenously distributing Au nanoparticles (AuNPs) on ZnO-CS matrix. The electrochemical performances of the designed electroeletrodes have been investigated using cyclic voltammetry (CV) and electrochemical impedance spectroscopy (EIS). Differential pulse voltammetry (DPV) was used to monitor the DNA hybridization event. The AuNPs/ZnO-CS film exhibited good conductor for accelerating the electron transfer, which led to obvious signal amplification and low detection limit for electrochemical sensing. Under optimum conditions, the peak currents of redox marker were linear with the logarithm of the concentrations of complementary DNA from 1.0×10^{-14} to 1.0×10^{-10} M with a detection limit of 2.0×10^{-15} M ($3\sigma/S$). The developed sensor also displayed high selectivity to differentiate one-base mismatched DNA. The excellent performance of biosensors is attributed to large surface-to-volume of ZnO superstructures and the synergistic effect of AuNPs and CS. The proposed approach provided a simple and reliable method for DNA detection and would open new opportunities for sensitive detection of other nucleic acids.

Keywords: flower-like 3-dimensional ZnO superstructures; Au nanoparticles; Chitosan; label-free DNA detection;

1. Introduction

DNA is the carrier of genetic information and plays a key role in the identification of specific species. The highly sensitive and selective detection of specific sequence of DNA is of great significance for the clinical diagnosis, pathogenic diseases, genetically modified organisms and environmental contamination, especially at very low physiological levels. Numerous techniques have been developed for the detection of DNA, of which the electrochemistry-based detection strategy is a powerful tool in various applications and is widely used in different fields of DNA detection because they have the potential for providing sensors of high sensitivity and low cost, suitable for on-site, decentralized testing. [1-5]

For electrochemical sensor construction, signal amplification is important to increase the detection sensitivity of DNA sensor, and some techniques have been applied for this goal such as utilizing multifunctional nanoparticles, exonuclease III-assisted target recycling amplification, enzyme labeling and sandwich-like analysis.[6-9] Among them, signal-amplification strategies based on different nanomaterials, such as metal nanoparticles, graphene, carbon nanosphere, and WS_2 nanosheets, etc., have the potential in realizing ultrasensitive DNA detection due to their unique properties including large specific surface area, very high surface activity, strong biological molecule absorb ability, good electro-conductivity and biocompatibility. [4, 5, 10] Especially, porous and layered nanomaterials with a crystalline frame work and high surface area have received significant research attention. [11, 12] By

rational designing and tailoring the layered or porous structure at the nanoscale level, the electron transportation can be significantly improved and the amount of loading objective molecules can be greatly enhanced, which makes it special suitable for ultrasensitive bioanalysis with signal amplification.

ZnO is a chemically and thermally stable n-type semiconductor material and has been investigated extensively over decades as luminescent materials, photocatalysts, solid state gas sensors, and solar cells. [13, 14] Nanostructured ZnO has attracted much attention not only for the fundamental scientific research but also for the potential application in the functional devices, and especially, nanostructured ZnO has attracted extraordinary attention in the fabrication of facile, biosafe, and low cost biosensors due to its large specific surface area, good biocompatibility, nontoxicity and high isoelectric point (IEP ~9.5) , which makes it appropriate for absorption of low IEP proteins or enzymes at pH 7.0 through electrostatic interactions. [15, 16]

Several electrochemical sensors based on nanostructure ZnO and ZnO nanocomposites for bioanalysis and environmental analysis have been developed. Das et al. have reported nanostructured ZnO films based DNA electrochemical biosensor for Tuberculosis detection. [16] Manvi Tak et al reported Flower-like ZnO nanostructure based electrochemical DNA biosensor for bacterial meningitis Detection. [17] Wang et al. reported gold nanoparticles, carbon nanotubes, and zinc oxide nanowires based sensitive DNA biosensor. [18]

Nanostructured ZnO has plenty of morphology, such as nanorods, [19] nanotubes, [20] nanowires, [21] nanoparticles, [22] nanonails, [23] nanocombs, [24] and nano-flake. [25]

Flower-like 3-dimensional (3D) ZnO superstructures has low density, good surface permeability, and extra high specific surface area, which is benefit to improve the loading amount of DNA probe. Chitosan (CS) is widely used to disperse nanomaterials due to its attractive properties including excellent film-forming ability, high water permeability, good adhesion and nontoxicity. Nanomaterial dispersed in CS has been reported to enhance electrochemical performance, ease of immobilization, biocompatibility and favorable microenviroment for fabrication of enzymatic biosensors. [26-29] In addition, CS has the abundant amino groups and could provide active sites for further AuNPs immobilization.

With high electrical conductivity, large specific surface and good biocompatibility, Au nanoparticles (AuNPs) have drawn extensive attention in the fabrication of nanoscale electronics, photonics, biochemical sensing, and catalytic devices because they can be used for promoting electrochemical transportation or as carriers for loading numerous signal tags. [30, 31] This noble metal nanoparticles based electrodes typically provide rapid response, good stability, electrocatalytic capability and reproducibility for the selected target detection.

In this work, flower-like 3D ZnO superstructures were synthesized by a simple one-step solution route using the trisodium citrate as shape-directing agent. The as-synthesized ZnO superstructures with an average diameter of 2-3 μm are assembled by large amounts of interleaving nanosheets with several nanometers in thickness and a well-crystalline structure, which have a high surface area (117.36 m^2 g^{-1}) and a large pore volume (0.50 cm^3 g^{-1}). A high sensitive electrochemical DNA

biosensor was developed for the detection of specific DNA sequences based on assembling DNA probe on flower-like 3D ZnO superstructures, CS and AuNPs modified glassy carbon electrode. The performance and factors influencing the nanoparticle-based assay were investigated and discussed. The contribution of this study was to develop an efficient nanolabel with highly amplified properties and a conductive sensing platform for the electrochemical assays. The developed approach provided a much simpler, faster and easier processing technique for DNA detection with high sensitivity and specificity than the previous works, [14-29] and would open new opportunities for sensitive detection of other nucleic acids.

2. Experimental

2.1. Apparatus

Scanning electron microscopy (SEM) observation was performed on a JEOL JSM-6480A scanning electron microscope. The crystalline structure of the samples was studied by X-ray diffraction (XRD) spectroscopy, using a Bruker Inc. (Germany) AXS D8 ADVANCE diffractometer (Cu Kα radiation). Transmission electron microscopy (TEM) observation was performed on a FEI Tecnai G2S-Twin transmission electron microscope (TEM) with an accelerating voltage of 200 kV. The Brunauer-Emmett-Teller (BET) surface area of the ZnO hollow sphere sample was tested using Quanta chrome NOVA 2000e sorption analyzer. Electrochemical measurements were performed on a CHI 660C Electrochemical Workstation (Shanghai, CH Instruments, China) with a conventional three-electrode system composed of a platinum wire as an auxiliary electrode, a saturated calomel electrode

(SCE) as a reference electrode and a 3-mm diameter GCE as a working electrode.

2.2. Reagents

Zinc acetate dihydrate, hexamine (HMTA), absolute ethanol and sodium citrate were obtained from China National Pharmaceutical Industry Corporation Ltd (Shanghai, China). Chitosan (CS) (M.W. 100,000-300,000, deacetylation degree ≥95%) and chloroauric acid ($HAuCl_4 \cdot 4H_2O$) were purchased from Sigma-Aldrich (St. Louis, USA). All chemicals used in this work were of analytical grade and were used without further purification. The sulphydryl modified 18-base oligonucleotides probe (probe ssDNA), target complementary sequence DNA (cDNA), one-base mismatched ssDNA, three-base mismatched ssDNA and noncomplementary sequence DNA (ncDNA) were synthesized by Shanghai Sangon Biological Engineering Technological Co. Ltd. (Shanghai, China). All DNA sequences were artificial sequences and were synthesized using standard phosphoramidite chemistry and purified using reversed phase HPLC. Their base sequences were list as below:

Capture probe DNA (S1): 5′-SH-$(CH_2)_6$-TCT TTG GGA CCA CTG TCG-3′;

Complementary target to S1 (S2): 5′-CGA CAG TGG TCC CAA AGA-3′;

One-base mismatch (underlined) target to S1 (S3): 5′-CGA CAG TGG TCC CAA C<u>C</u>GA-3′;

Three-base mismatch (underlined) target to S1 (S4): 5′-CGA CA<u>A</u> TGG <u>C</u>CC CAA C<u>C</u>GA-3′;

Noncomplementary target to S1 (S5): 5′-GCA TCG AGC GAG CAC GTA-3′.

2.3. Synthesis of Au nanoparticles

The AuNPs with about 3.5 nm diameter were prepared according to the reference. [32] Briefly, a 20 mL aqueous solution containing 2.5×10^{-4} M $HAuCl_4\cdot4H_2O$ and 2.5×10^{-4} M trisodium citrated was prepared in a beaker. Next, 0.6 mL ice-cold $NaBH_4$ solution (0.1 M) was quickly added to the above solution under stirring. The solution turned pink immediately with the adding $NaBH_4$, indicating the formation of AuNPs. Upon continued stirring and cooling down, the AuNPs solution was obtained and stored in brown glass bottles at 4 °C before use.

2.4. Synthesis of flower-like 3D ZnO superstructures

The preparation and the growth mechanism of flower-like 3D ZnO superstructures have been studied in our previous work. [33] In a typical synthesis, an equimolar ratio of zinc acetate dihydrate (25 mM) and HMTA (25 mM) was dissolved into 50 mL deionized water, and 5 mM trisodium citrate was then added and ultrasonically dispersed for 20 min at room temperature. After that, the mixture was transferred into a 100 mL Teflon-lined stainless steel autoclave and heated at 90 ℃ for 10 h. After cooling, the flower-like 3D ZnO superstructures were collected by filtration, washed with distilled water and absolute ethanol for several times, and dried in vacuum at 60 ℃ for 24 h.

2.5. Fabrication of DNA sensor based on ZnO superstructures

The glassy carbon electrode (GCE) (3 mm in diameter) was polished carefully with 0.05 μm alumina slurry, and then sonicated in ethanol and water, respectively. The electrode was dried in the nitrogen atmosphere. 1 mg ZnO superstructures and 1 mg CS was dispersed in 1 mL acetic acid (1%) solution with ultrasonication for 30

min to get a homogenous suspension. Then 5 μL ZnO-CS suspensions was applied on the pretreated GCE surface and naturally dried in the air to form the modified electrode, which was denoted as ZnO-CS/GCE. Afterwards, the dried ZnO-CS/GCE was exposed to AuNPs for 12 h following with rinsed with deionized, ultrafiltered water, dried in air to obtain AuNPs/ZnO-CS/GCE.

The thiolated probe ssDNA was immobilized by directly applying 10 μL S1 (1 μM) on the surface of AuNPs/ZnO-CS/GCE for 12 h to obtain modified electrode S1/AuNPs/ZnO-CS/GCE. Subsequently, the S1/AuNPs/ZnO-CS/GCE was washed with 0.1 wt% sodium dodecyl sulfate (SDS) in phosphate buffer solution (PBS, pH 7.0) to eliminate the non-specific adsorbed probe ssDNA molecules. In order to eliminate the non-specifically adsorbed ssDNA molecules and hold a good orientation of probe ssDNA for its good recognition ability, the resultant electrode was then subjected to 1 mM 6-mercaptohexanol (MCH) treatment for 1 h. The hybridization

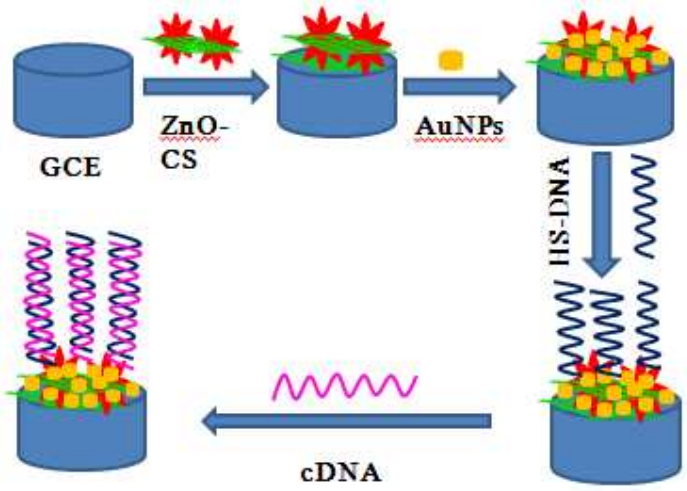

Scheme 1. Schematic diagram of the electrochemical DNA biosensor.

reaction of complementary target ssDNA sequence and S1/AuNPs/ZnO-CS/GCE was performed by applying 10 μL complementary target ssDNA sequence on the S1/AuNPs/ZnO-CS/GCE at 30 °C for 60 min. Finally, the hybridized electrode S2-S1/AuNPs/ZnO-CS/GCE was washed with 0.1 wt% SDS in PBS (pH 7.0) to remove the unhybridized complementary target ssDNA sequence. The schematic diagram of the stepwise procedure of the DNA biosensor fabrication was shown in Scheme 1.

2.6. Electrochemical detection

The electrochemical responses of the $[Fe(CN)_6]^{3-/4-}$ on the different electrode surfaces were measured by the cyclic voltammetry (CV) and differential pulse voltammetry (DPV) in 0.1 M PBS (pH 7.0) containing 0.1 M KCl. The instrumental parameters of DPV were as follows: pulse amplitude 0.005 V, pulse width 0.05 s and pulse period 0.2 s. Electrochemical impedance spectroscopy (EIS) experiment was performed in a 10.0 mL aqueous solution containing 1.0 mM $[Fe(CN)_6]^{3-/4-}$ and 0.1 M KCl at a potential of 0.2 V over the frequency range from 0.1 Hz to 10^4 Hz, using an amplitude of 5 mV.

3. Results and discussion

A highly sensitive electrochemical DNA sensor was constructed by using high specific surface area ZnO superstructures modified electrode to anchor Au nanoparticles (AuNPs), which were further coupled with capture ssDNA sequences to amplify the electrochemical signal of hybridization reaction. The structure and surface

morphology of the ZnO superstructures have been studied by means of X-ray diffraction (XRD) analysis, scanning electron microscopy (SEM) and transmission electron microscopy (TEM). The electrochemical performances of the designed electroeletrodes have been investigated using cyclic voltammetry (CV) and electrochemical impedance spectroscopy (EIS). Differential pulse voltammetry (DPV) was used to monitor the DNA hybridization event.

3.1. Characterization of ZnO superstructures

Fig. 1A and 1B display the SEM images of the ZnO superstructures. A low-magnification view of the products shown in Fig. 1A reveals the product consists of relatively uniform, well-dispersed flower-like structure with an average diameter of 2-3 μm. The magnified SEM image in Fig. 1B shows that the micro-flower exhibits a hierarchical structure. Interestingly, the flower-like 3D structures are assembled by a large number of nanosheets with an average thickness of several nanometers. The nanosheets intersect with each other, which results in a net-like structure with porous surfaces. The as-synthesized ZnO superstructures were further characterized by TEM.

As shown in Fig. 1C, the sample shows the typical thin layers folded and tangled together structure to form 3D superstructures, which is helpful to increase the specific surface area of the product. Furthermore, the overlapping or coalescing of the ZnO nanosheets in the 3D superstructures would form an interconnected conducting network, and provided a feasible pathway for electron transfer. These properties are very beneficial to the construction of an excellent electrochemical sensing and electrocatalytic platform.

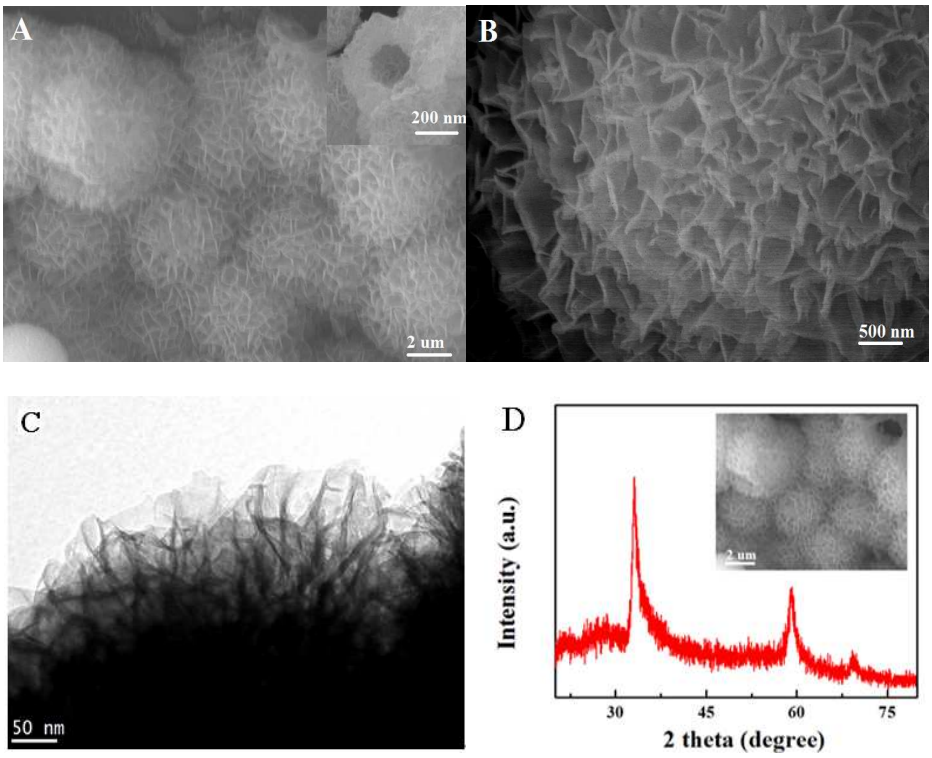

Fig. 1. FESEM images, TEM image and XRD pattern of ZnO superstructures. (A) low magnification FESEM image; (B) high-magnification FESEM image; (C) TEM image; (D) XRD pattern

The XRD pattern of ZnO superstructures was recorded in Fig. 1D. The strong diffraction peaks are observed which are indexed to a ZnO phase (PDF # 21-1486).

For the sake of further studying the porosity and textural properties of the as-prepared porous ZnO superstructures, the N_2 adsorption-desorption measurement was conducted. As seen from Fig. 2a, the adsorption-desorption N_2 isotherm of the products presents the typical IV sorption behavior with the profile of a hysteresis loop according to the classification of international union of pure and applied chemistry

classification, suggesting its typical porous structure. An abrupt increase in desorption volume is observed and located in a P/P_0 value greater than 0.55. This sharp increase is generally associated with capillary condensation, which means the good homogeneity and small pore size of the sample. The BET (Brunauer-Emmett-Teller) surface area and the pore volume are found to be 117.36 m^2g^{-1} and 0.50 cm^3 g^{-1} respectively. Furthermore, the pore-size distribution, which is obtained from the Barrett-Joyner-Halenda method by calculation from the desorption branch of the isotherm, shows the porous ZnO superstructures with an average pore diameter of 18.2 nm. The large specific surface area and the thin layer stacking structure of flower-like 3D ZnO superstructures make it attractive for electrochemical sensor development.

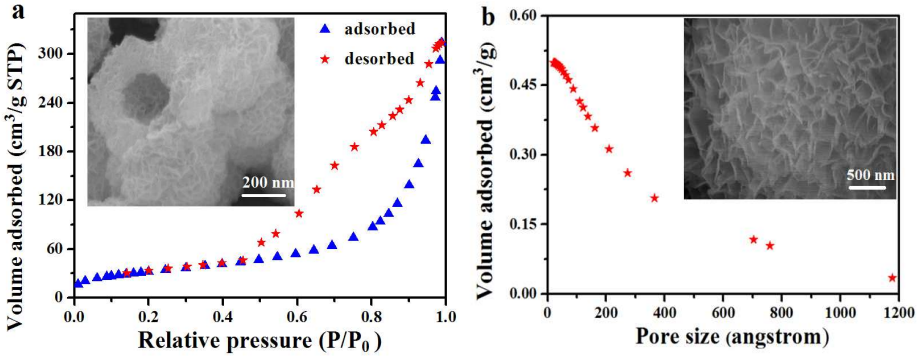

Fig. 2 Nitrogen adsorption-desorption isotherm (a), BJH pore size distribution curve (b)

3.2. Electrochemical characterization

Fig. 3A depicts the CV behavior of the GCE at different stages of modifications

made in the presence of 1 mM $[Fe(CN)_6]^{3-/4-}$ and 0.1 M KCl in PBS at a scan rate 100 mV s^{-1}. It can be observed that the CV of bare GCE (curve a) shown a well-defined reversible redox behavior of $[Fe(CN)_6]^{3-/4-}$ with oxidation peak current I_{pc} of 26 μA and ΔE_p (E_{pa}-E_{pc}) of 60 mV. After deposition of ZnO-CS film onto the GCE surface, an apparent increase in the peak current of $[Fe(CN)_6]^{3-/4-}$ (I_{pc}: 33 μA) is observed (curve b). The observed increase is attribute to the large surface area of ZnO superstructures which enhance the diffusion of $[Fe(CN)_6]^{3-/4-}$ towards the electrode surface through electrostatic interactions and the positivity charge of $-NH_3^+$ groups in CS. Furthermore, dispersion of the Au nanoparticles onto the ZnO-CS film greatly enhances the peak current and the reversible process (I_{pc}: 42 μA, ΔE_p: 40 mV) (curve c), indicating more efficient electron transfer which is due to the excellent conductivity of AuNPs. The reversibility and peak current of the $[Fe(CN)_6]^{3-/4-}$ decreased after the capture probe S1 was immobilized on the AuNPs/ZnO-CS/GCE (I_{pc}: 28 μA, ΔE_p: 70 mV) (curve d) . This was due to electrostatic repulsion between the negatively charged HS-ssDNA and $[Fe(CN)_6]^{3-/4-}$. After the S1/AuNPs/ZnO-CS/GCE hybridized with the complementary target DNA S2, the I_{pc} decreases to 18 μA and ΔE_p increases to 75 mV (curve e), indicating the introduction of complementary DNA increased the negative charge responsible for the increased repellence of redox species. These results proved that the biosensor worked indeed as described in the principle scheme.

Further, the charge transport properties of the composite film modified electrodes were characterized by electrochemical impedance spectroscopy (EIS). In EIS, the

semicircle diameter could represent the electron-transfer resistance (R_{et}), which dominates the electron transfer kinetics of the redox probe at the electrode interface/electrolyte interface. The data could be fitted with an equivalent circuit (inset in Fig. 3B). GCE displays a small semicircle at high frequencies and a linear Nyquist plot at low frequencies (curve a), suggesting a low R_{et} (300 Ω) to redox probe $[Fe(CN)_6]^{3-/4-}$. When ZnO-CS composites are immobilized on the bare GCE, the R_{et} value decreases to about 230 Ω (curve b), indicating the ZnO-CS composite acted as an accelerator for electron transfer of $[Fe(CN)_6]^{3-/4-}$. When AuNPs are further immobilized on the ZnO-CS/GCE, the R_{et} greatly decreases and exhibits almost a line (curve c), indicating that ZnO-CS composites and AuNPs present on the surface of GCE could greatly enhance the conductivity and facilitated the electron transfer between solution and electrode interface. Moreover, these results also indicated that ZnO-CS composites and AuNPs were successfully modified on the surface of GCE. The R_{et} greatly increased to about 1500 Ω (curve d) when the thiolated probe ssDNA S1 was immobilized onto the AuNPs/ZnO-CS/GCE, suggesting the successful immobilization of the capture probe DNA on the electrode. After S1/AuNPs/ZnO-CS/GCE hybridized with target DNA, the R_{et} obviously increased to about 3000 Ω (curve e), indicating the formation of double-stranded structure.

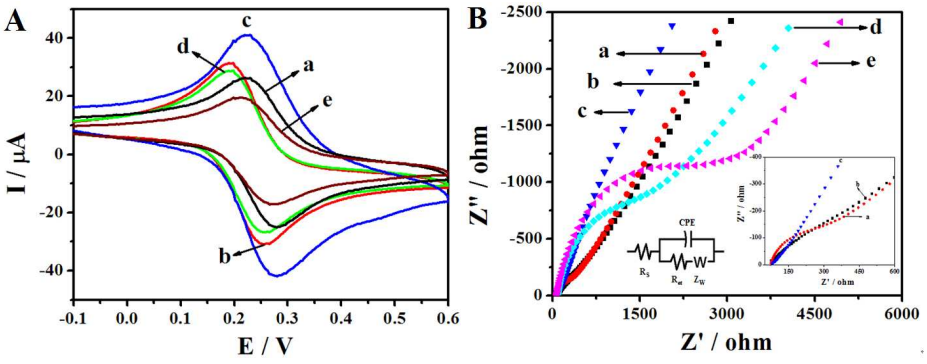

Fig. 3 CVs (A) and EIS (B) of different electrodes in 1.0 mM $[Fe(CN)_6]^{3-/4-}$ containing 0.1 M KCl. The frequency range is from 0.1 to 10^4 Hz at the formal potential of 0.2 V. (a) bare GCE, (b) ZnO-CS/GCE, (c) AuNPs/ZnO-CS/GCE, (d) S1/AuNPs/ZnO-CS/GCE, (e) S2-S1/AuNPs/ZnO-CS/GCE; Inset is the Randles circuit model for the modified electrodes: R_S, electrolyte solution resistance; R_{et}, element of interfacial electron transfer resistance; Z_W, Warburg impedance resulting from the diffusion of ions.

3.3. Optimization of the experiment conditions

To obtain excellent analytical performance, different experimental conditions were optimized (Fig. 4A-C). The ssDNA (S1) reacted with AuNPs/ZnO-CS/GCE by the Au-thiol chemistry, so the effect of incubation time of S1 and AuNPs/ZnO-CS/GCE was studied in order to obtain the larger signal readout. Fig. 4A shows the DPV response of the $[Fe(CN)_6]^{3-/4-}$ changed with the incubation time varied from 0 to 18 h. The peak currents decrease significantly with increasing incubation time from 0 up to 12 h, and then reached a platform, indicating the most probe ssDNA

have been immobilized on the electrode after 12 h. So this time was used in the further experiments.

The hybridization time and temperature of the capture probe DNA and the target DNA on the peak current of $[Fe(CN)_6]^{3-/4-}$ were also studied. As shown in Fig. 4B, the peak current obviously decreases with increasing the hybridization time from 0 to 60 min, and remains stable after 60 min, indicating that the hybridization reaction is completed. Then 60 min was chosen as hybridization time to achieve a balance between high sensitivity and assay time. The effect of hybridization temperature on the DPV response was tested in the range of 20-60 °C. As shown in Fig. 4C, the lowest peak current occurred at 30 °C. Therefore, the hybridization temperature was chosen as 30 °C.

DNA hybridization efficiency at surfaces is a sensitive function of surface density of immobilized DNA capture probes. We thus applied different concentrations of DNA capture probe varying probe concentration on AuNPs/ZnO-CS/GCE and then evaluated the DPV response (Fig. 4D). It is found that the lowest peak current is realized at a probe concentration of 1 μM. The signal increased as the probe concentration exceeds 1 μM. The reason might be that the hybridization efficiency decreases at high probe concentration because of steric hindrance effect. So, 1 μM DNA capture probe was used in the biosensor preparation.

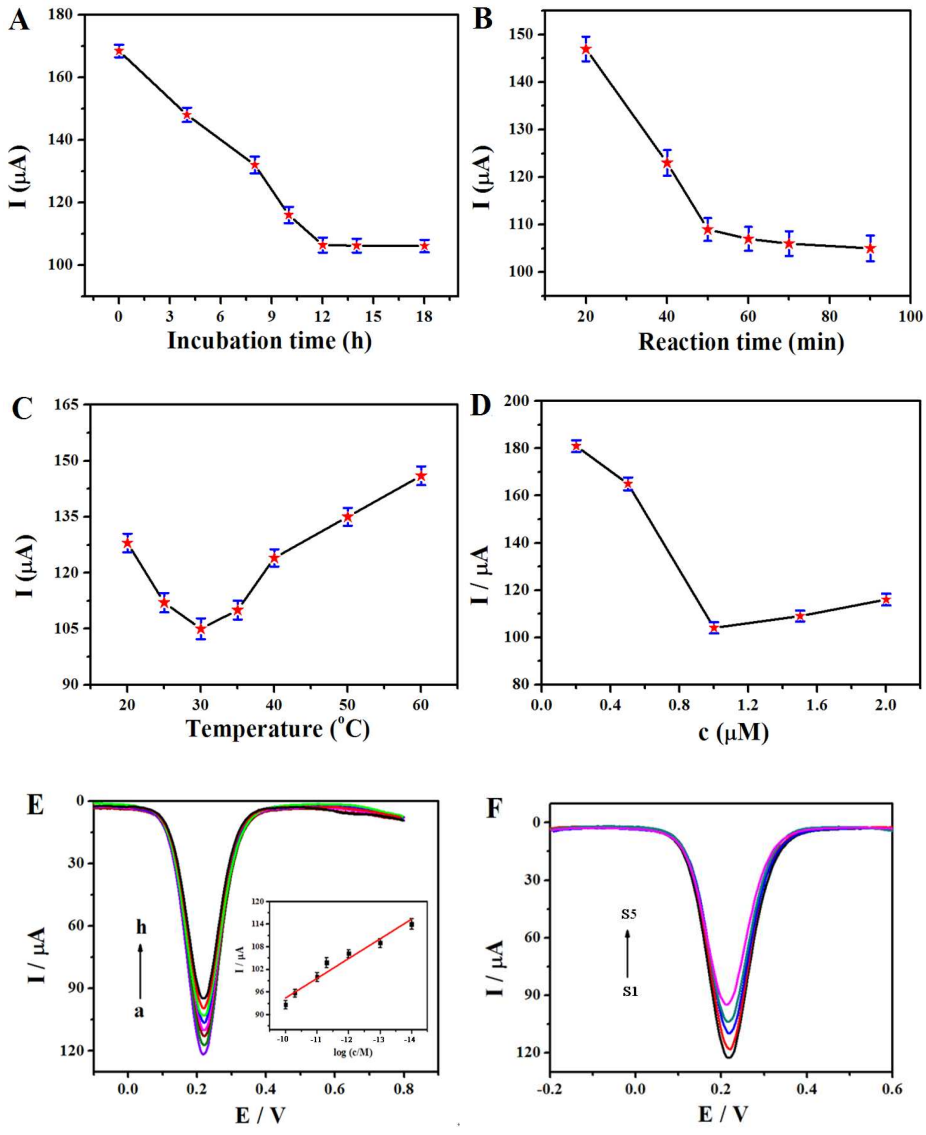

Fig. 4 The effect of the incubation time (A), reaction time (B), reaction temperature (C) and the concentration of probe DNA S1 (D) on the peak current in CVs in 1.0 mM $[Fe(CN)_6]^{3-/4-}$ containing 0.1 M KCl; (E) the DPVs of the proposed sensor after incubation in different concentrations of target ssDNA solution (from a to h): 0 0.00001, 0.0001, 0.001, 0.005, 0.01, 0.05, and 0.1 nM under the optimal conditions. The inset is the calibration plots for target ssDNA with the proposed DNA biosensor. (F) DPVs of 1 mM $[Fe(CN)_6]^{3-/4-}$ on S1/AuNPs/ZnO-CS/GCE (1) and its

hybridization with 1.0 nM different ssDNA sequence: non-complementary sequence (2), three-based mismatch sequences (3), single-based mismatch sequences (4), and complementary sequences (5).

3.4. DNA hybridization detection at AuNPs/ZnO-CS composite

Under optimal conditions, the sensitivity of sensor was performed by DPV measurement. Fig. 4E depicts DPV curves for varied concentrations of target DNA. The inset of Fig. 4E shows the peak current decreased with the increasing concentration of target DNA. There was a good linear relationship between the peak current and the logarithm of the target DNA concentration in the range from 0.1 nM to 0.01 pM. The linear calibration equation was i_p (μA) = 47.36 – 5.23×log c (i_p is the

Table 1 Comparison between the proposed sensor and other sensor for DNA detection.

Electrodes	Analytical technique	Linear range (nM)	LOD (pM)	References
GO-CS/ITO	DPV	0.0001-50	0.1	[34]
Gr/polyaniline/GCE	DPV	0.0001-700	0.032	[35]
FePt/CNTs/GCE	EIS	0.001-1000	0.21	[36]
PAN-nanoZrO_2/PTyr	EIS	0.0001-1000	0.0268	[37]
CeO_2/CS/GCE	DPV	0.0159-116	10	[38]
AuNPs-ATPGO/GCE	EIS	0.0001-100	0.02	[39]
AuNPs/ZnO-CS/GCE	DPV	0.00001-0.1	0.002	This work

peak current and c is the concentration of the target DNA in M) and the correlation coefficient R = 0.9847. The detection limit was estimated to be 0.002 pM estimated as three times the standard deviation of the blank sample measurements. The performance of the fabricated DNA biosensor has also been compared with those reported in the literatures that have used nanostructured materials for the DNA immobilization layer and the results are shown in Table 1. Compared with some special instrumental methods like PCR, it is still less sensitive, while the proved detection is relatively simple, of low cost, and has significant sensitivity.

3.5. Detection specificity of biosensor

In order to evaluate the selectivity of this biosensor, we investigated four different DNA sequences (1.0 nM L^{-1}) including perfectly complementary targets (S2), one-base mismatched strands (S3), three-base mismatched strands (S4) and non-complementary strands (S5). Fig. 4F depicts the DPV respond of different targets. Herein, ΔI is defined as $I-I_0$ (I is the peak current in the presence of target and I_0 is the peak current in the absence of target). It is found that a very low ΔI was observed for the S5, since no successful hybridization occurred due to the sequence mismatch between the modified S1 and S5. However, further increase of ΔI was obtained for S4, S3 and S2. These results demonstrated that the electrochemical DNA biosensor was able to detect effectively a target with high specificity, and had great potential for single nucleotide polymorphism analysis.

3.6. The stability and reproducibility of DNA sensor

The stability of the S1/AuNPs/ZnO-CS/GCE was investigated after 15 days

storage at 4 ℃ and was further used to hybridize with the target ssDNA sequence (0.05 nM) and 94.3% of the initial DPV respond was observed. This good stability was mainly attributed to the AuNPs/ZnO-CS composite film which possessed excellent environmental and chemical stability. The reproducibility of five different biosensors constructed in the same manner, for 0.05 nM target DNA, showed the response of peak current values with a relative standard deviation (RSD) value of 4.6%, indicating the fabrication procedure of the developed biosensor was reliable.

4. Conclusion

In this work, flower-like 3-dimensional ZnO superstructure was prepared by a simple one-step solution route, and a novel electrochemical sensor for detection of DNA hybridization was constructed based on ZnO superstructures-chitosan and Au nanoparticals composite modified glassy carbon electrode. The as-prepared DNA sensor was sensitive, selective for target DNA with a low detection limit down to 0.002 pM. The ZnO superstructures-chitosan and Au nanoparticals composite film was proved to be a good sensing platform which can offer a strategy to enhance the electrochemical performance and be used as the nanomaterial to construct sensitive sensors for determination of DNA hybridization. Furthermore, the good reproducibility and detection sensitivity may expand the potential of ZnO superstructures as an entirely new and flexible electrochemical material for signal-amplification detection of biomolecules.

Acknowledgments

The authors are grateful for the financial support provided by National High

Technology Research and Development Program of China (No. 2012AA02A404), National Natural Science Foundation of China (U1304214, No. 51173146), basic research fund of Northwestern polytechnical university (JC20120248) and the Natural Science Foundation of Henan Province (nos. 132300410406).

References

[1] Y. Guo, J.H. Chen, G.N. Chen, Sensor. Actuators B, 184 (2013) 113.

[2] Y.W. Hu, S.C. Hua, F.H. Li, Y.Y. Jiang, X.X. Bai, D. Li, L. Niu, Biosens. Bioelectron., 26 (2011) 4355.

[3] X.M. Meng, M.R. Xu, J.Y. Zhu, H.S. Yin, S.Y. Ai, Electrochim Acta, 71 (2012) 233.

[4] K.J. Huang., Y.J. Liu, H.B. Wang, T. Gan, Y.M. Liu, L.L. Wang, Sensor. Actuators B, 191 (2014) 828.

[5] M. Bhuvana, J.S. Narayanan, V. Dharuman, W. Teng, J.H. Hahn, K. Jayakumar, Biosens. Bioelectron. , 41 (2013) 802.

[6] H. Gao, X. Jiang, Y.J. Dong, W.X. Tang, C. Hou, N.N. Zhu, Biosens. Bioelectron. , 48 (2013) 210.

[7] C.H. Luo, H. Tang, W. Cheng, L. Yan, D.C. Zhang, H.X. Ju, S.J. Ding, Biosens. Bioelectron. , 48 (2013) 132.

[8] R.M. Kong, Z.L. Song, H.M. Meng, X.B. Zhang, G.L. Shen, R.Q. Yu, Biosens. Bioelectron. , 54 (2014) 442.

[9] X.Y. Dong, X.N. Mi, L. Zhang, T.M. Liang, J.J. Xu, H.Y. Chen, , Biosens. Bioelectron. , 38 (2012) 337.

438 [10] H.F. Dong, Z. Zhu, H.X. Ju, F. Yan, Biosens. Bioelectron. , 33 (2012) 228.

439 [11] Z.M. Baccar, D. Caballero, R. Eritja, A. Errachid, Electrochim. Acta, 74 (2012)
440 123.

441 [12] G.G. Rong, A. Najmaie, J.E. Sipe, S.M. Weiss, Biosens. Bioelectron., 23 (2008)
442 1572.

443 [13] X.H. Chen, X.Y. Jing, J. Wang, J.Y. Liu, D.L. Song, L.H. Liu, Superlattice.
444 Microst, 63 (2013) 204.

445 [14] F. Muharnmad, M.Y. Guo, W.X. Qi, F.X. Sun, A.F. Wang, Y.J. Guo, G.S. Zhu,
446 J. Am. Chem. Soc., 133 (2011) 8778.

447 [15] Y.T. Wang, L. Yu, J. Wang, L. Lou, W.J. Du, Z.Q. Zhu, H. Peng, J.Z. Zhu, J.
448 Electroanal. Chem., 661 (2011) 8.

449 [16] M. Das, G. Sumana, R. Nagarajan, B. D. Malhotra, Thin Solid Films, 519 (2010)
450 1196

451 [17] M. Tak, V. Gupta, M. Tomar, http://dx.doi.org/10.1016/j.bios.2014.03.036

452 [18] J. Wang, S. Li, Y. Zhang, Electrochim. Acta, 55 (2010) 4436

453 [19] G.N. Dar, A. Umar, S.A. Zaidi, S. Baskoutas, S.H. Kim, M. Abaker, A.
454 Al-Hajry, S.A. Al-Sayari, Sci. Adv. Mater. 3 (2011) 901.

455 [20] S.M.U. Ali, M. Kashif, Z.H. Ibupoto, M.F. Alam, U. Hashim, M. Willander,
456 Micro Nano Lett. 6 (2011) 609.

457 [21] S.M. Usman Ali, O. Nur, M. Willander, B. Danielsson, Sensor. Actuators B, 145
458 (2010) 869.

[22] Z.H. Dai, G.J. Shao, J.M. Hong, J.C. Bao, J. Shen, Biosens. Bioelectron. 24 (2009) 1286.

[23] Y. B. Hahn, Korean J. Chem. Eng. 28 (2011) 1797.

[24] J.X. Wang, X.W. Sun, A. Wei, Y. Lei, X.P. Cai, C.M. Li, Z.L. Dong, App. Phys. Lett. 88 (2006) 233106.

[25] A. Fulati, S.M. Usman Ali, M.H. Asif, N.H. Alvi, M. Willander, C. Brannmark, P. Stralfors, S.I. Borjesson, F. Elinder, B. Danielsson, Sensor. Actuators B 150 (2010) 673.

[26] S.J. Ling, R. Yuan, Y.Q. Chai, T.T. Zhang, Bioprocess Biosyst. Eng. 32 (2009) 407.

[27] B. Batra and C.S. Pundir, Biosens. Bioelectron. 47 (2013) 496.

[28] C. Shan, H. Yang, D. Han, Q. Zhang, A. Ivaska, L. Niu, Biosens. Bioelectron., 25 (2009) 1070.

[29] H. Bao, Y. Pan, Y. Ping, N.G. Sahoo, T. Wu, L. Li, J. Li, L.H. Gan, Small, 7 (2011) 1569.

[30] H. Yin, Y. L. Zhou, H. X. Zhang, X. M. Meng, S. Y. Ai, Biosens. Bioelectron., 1 (2012) 247.

[31] S. H. Hou, Z.M. Ou, Q. Chen, B.Y. Wu, Biosens. Bioelectron., 1 (2012) 44

[32] Y. Jiang, H. Zhao, N.N. Zhu, Y.Q. Lin, P. Yu, L.Q. Mao, Angew. Chem. Int. Edit. 47 (2008) 8601.

[33] L. X. Fang, B. L. Zhang, W. Li, X. J. Li, T. J. Xin, Q. Y. Zhang, RSC Adv., 4 (2014) 7167

481 [34] A. Singh, G. Sinsinbar, M. Choudhary, V. Kumar, R. Pasrich, H.N. Verm, P.
482 Surinder, K. A. Singh, Sensor. Actuators B, 185 (2013) 675.
483 [35] M. Du, T. Yang, X. Li, K. Jiao, Talanta, 88 (2012) 439.
484 [36] W. Zhang , P. S. Zong, X. W. Zheng , L. B. Wang, Biosens. Bioelectron., 42
485 (2013) 481.
486 [37] J. Yang, X. Wang, H. Shi, Sensor. Actuators B, 162 (2012) 178.
487 [38] K.J. Feng, Y.H. Yang, Z.J. Wang, J.H. Jiang, G.L. Shen, R.Q. Yu, Talanta, 70
488 (2006) 561.
489 [39] V. K. Gupta, M. L. Yola, M. S. Qureshi, A. O. Solak, N. Atar, Z. Üstündağ,
490 Senso. Actuators B, 188 (2013) 1201.